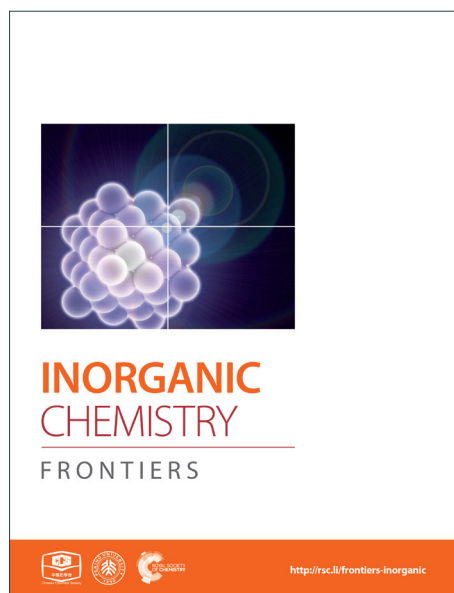
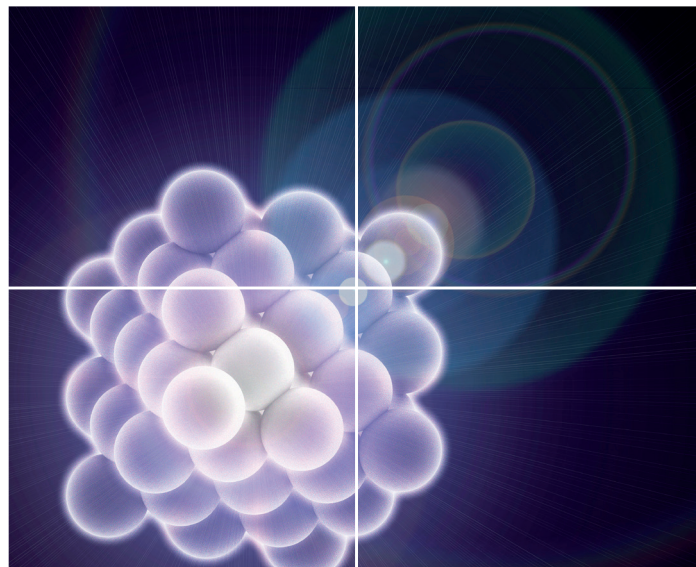


INORGANIC CHEMISTRY

FRONTIERS

Accepted Manuscript



This is an *Accepted Manuscript*, which has been through the Royal Society of Chemistry peer review process and has been accepted for publication.

Accepted Manuscripts are published online shortly after acceptance, before technical editing, formatting and proof reading. Using this free service, authors can make their results available to the community, in citable form, before we publish the edited article. We will replace this *Accepted Manuscript* with the edited and formatted *Advance Article* as soon as it is available.

You can find more information about *Accepted Manuscripts* in the [Information for Authors](#).

Please note that technical editing may introduce minor changes to the text and/or graphics, which may alter content. The journal's standard [Terms & Conditions](#) and the [Ethical guidelines](#) still apply. In no event shall the Royal Society of Chemistry be held responsible for any errors or omissions in this *Accepted Manuscript* or any consequences arising from the use of any information it contains.

ARTICLE

Nickel hydroxide-nickel nano hybrids indirectly from coordination microfibers for high-performance supercapacitor electrodes

Cite this: DOI: 10.1039/x0xx00000x

Junhong Zhao,^a Junzhi He,^a Mengjun Sun,^a Meijiao Qu,^a and Huan Pang^{*a,b}Received 00th January 2014,
Accepted 00th January 2014

DOI: 10.1039/x0xx00000x

www.rsc.org/

Nickel nanowire foams are primarily synthesized by calcinations of dimethylglyoxime nickel microfibers in Ar gas. Moreover, mesoporous nickel hydroxide-nickel nano hybrids are successfully obtained via oxidation of Ni nanowire foams in the alkaline H₂O₂ aqueous solution. Due to the mesoporous structure of nickel hydroxide and the high conductivity of central Ni metal, electrodes assembled with nickel hydroxide-nickel nano hybrids show the highly accessible surface-interface site and high conductivity, which are successfully applied as high-performance supercapacitor electrodes.

1. Introduction

Nowadays, more and more attention has been paid to various power source devices for clean and efficient energy storage, such as Li-ion batteries, supercapacitors, fuel cells and so on.¹⁻⁵ In recent years, the electrochemical capacitors have received much attention due to their higher power density and longer cycle life compared to secondary batteries and higher energy density than conventional electrical double-layer capacitors.⁶⁻⁸ In particular, electrochemical capacitors based on hydrous ruthenium oxides exhibit much higher specific capacitance than conventional carbon materials and better electrochemical stability than electronically conducting polymer materials.^{9,10} Nevertheless, the high cost of this noble metal material limits its commercialization. Hence, much effort has been aimed at searching for alternative inexpensive electrode materials with good capacitive characteristics, such as Ni-based materials,¹¹⁻²⁰ Co-based materials²¹⁻³¹ and Mn-based materials,³²⁻³⁹ etc. They show high specific capacitance and energy density, which can be ascribed to Faradic redox reactions.

However, the poor electrical conductivity of metal oxides leads to lower electron transport rates. In order to solve this issue, recently there are a number of efforts on improving the electrical conductivity. Many strategies are tried and two prove effective: a) One is to incorporate directly electrochemically active materials are incorporated directly into good conductive carbon materials (activated carbon,⁴⁰ mesoporous carbon,⁴¹ carbon nanotubes,^{42,43} or graphene⁴⁴). However, it always results in a decrease in the conductivity of the carbon materials when some functional groups are introduced onto the carbon materials for better bonding with the pseudocapacitor materials; b) The other one is to construct a pseudocapacitor material-conductive matrix hybrid nanostructure⁴⁵⁻⁴⁹. The matrix with a porous conductive network improves the electron transport rate leading to an enhanced supercapacitor performance. For instance, Chen et al.⁴⁵ synthesized a MnO₂-gold matrix hybrid structure for supercapacitors. Xiao et al.⁴⁶ constructed monolithic NiO-Ni matrix composites for supercapacitors by

mechanically compacting Ni powder to produce thin pellet disks, followed by a subsequent low-temperature annealing process.

Recently, Ni(OH)₂/nickel foam (NF) composites have been focused on preparing.⁵⁰⁻⁵² Such as, a hydrothermal method is applied to deposit ultrathin primary nanowalls of Ni(OH)₂ on NFs, and the composites show a capacitance higher than the theoretical value.⁵⁰ What's more, porous and 3D nanostructured Ni(OH)₂ is electrodeposited on NFs to synthesize the composites.⁵¹ And the Ni(OH)₂/NF composites also are prepared by chemical bath deposition.⁵² The spike-piece-structured Ni(OH)₂ multilayer nanoplate arrays on nickel foams are directly synthesized by a facile hydrothermal method, which shows high-performance for energy storage.⁵³ Ni(OH)₂ nanoflakes array on Ni foam were fabricated as a binder-free electrode material for high performance supercapacitors.⁵⁴ Though these important developments have been done, there are no reports for synthesis of Ni(OH)₂ nanoflakes on Ni micro/nanofibers and corresponding application of supercapacitors.

Dimethylglyoxime (CH₃(C=NOH)₂CH₃, DMG) is a common organic precipitant for Ni²⁺ in industry.⁵⁵ Herein, the red precursor was easily synthesized by mixing dimethylglyoxime and Ni(OAc)₂ in aqueous solution with vigorous stirring (see Experimental details and **Figure S1**). X-ray diffraction (XRD) analysis and scanning electron microscopy (SEM) observation confirm that the obtained product is Ni(DMG)₂, which has a one-dimensional morphology, with an average diameter of ~1000 nm (corresponding XRD pattern and SEM image are shown in **Figure S2**, and **S3**). Dimethylglyoxime can chelate with Ni²⁺ ion to form a square planar configuration with Ni²⁺ in the centre. The central metal Ni²⁺ ions interact strongly with the adjacent molecular and the square planes stack face-to-face, resulting in a one-dimensional columnar structure.⁵⁶ This inherent columnar structure would lead to the formation of Ni(DMG)₂ microfibers. More importantly, we have successfully synthesized porous Ni nanowire foams (denoted **P1**) by the calcination of Ni(DMG)₂ microfibers in Ar gas. The obtained Ni nanowire foams are further oxidized in alkaline H₂O₂ aqueous solution under hydrothermal condition. Thus the mesoporous nickel

hydroxide-nickel ($\text{Ni}(\text{OH})_2\text{-Ni}$) nanohybrids (denoted **P2**) have successfully been obtained. The mesoporous structure and high surface area of $\text{Ni}(\text{OH})_2$ offer many nanochannels for the electrolyte or ions, and the central Ni improves the conductivity of the as-prepared electrode. At a relatively low current density of 1.25 A g^{-1} , the mesoporous $\text{Ni}(\text{OH})_2\text{-Ni}$ nanohybrid electrode delivers a high capacitance of 1793 F g^{-1} . Even when the current density is increased by 10 fold, namely 12.5 A g^{-1} , the values remain as high as 850 F g^{-1} .

2. Experimental methods

2.1 Materials preparation

Synthesis of $\text{Ni}(\text{DMG})_2$ microfibers: Firstly, 0.25 g dimethylglyoxime were added into 100 mL ethanol with stirring. And then 0.15 g $\text{Ni}(\text{CH}_3\text{COO})_2 \cdot 4\text{H}_2\text{O}$ were added into above solution and stirred them for 30 min. After that, red precipitates were obtained. The precipitates were centrifuged, washed with deionized water as well as ethanol, and dried at room temperature.

Synthesis of Ni nanowire foams: The as-prepared $\text{Ni}(\text{DMG})_2$ microfibers were heated from room temperature to 500°C at Ar atmosphere with a heating rate of 1°C min^{-1} , and maintained at 500°C for 30 min.

Synthesis of mesoporous $\text{Ni}(\text{OH})_2\text{-Ni}$ nanohybrids: 0.02 g Ni nanowire foams, 0.2 g NaOH, and 20 mL 30% H_2O_2 solution were put in a Teflon-lined stainless-steel autoclave, and heated at 180.0°C for 18 h. After the hydrothermal process, the product was easily separated. Then the final product was thoroughly washed with deionized water and ethanol to remove ions possibly remaining in the final products, and dried in air.

2.2 Characterizations

The morphology of the as-prepared samples was observed with a JEOL-6701F field-emission scanning electron microscope (FESEM) at an acceleration voltage of 5.0 kV. The phase analyses of the samples were performed by X-ray diffraction (XRD) on a Rigaku-Ultima III with $\text{Cu K}\alpha$ radiation ($\lambda = 1.5418 \text{ \AA}$). Nitrogen adsorption-desorption measurements were performed on a Gemini VII 2390 Analyzer at 77 K using the volumetric method. The specific surface area was obtained from the N_2 adsorption-desorption isotherms and was calculated by the Brunauer-Emmett-Teller (BET) method. Transmission electron microscopy (TEM) images and HRTEM, STEM images were captured on the FEI Tecnai G2 F20 S-TWIN instrument microscopy at an acceleration voltage of 200 kV.

2.3 Electrochemical measurements

Electrochemical study on mesoporous $\text{Ni}(\text{OH})_2\text{-Ni}$ nanohybrids electrodes were carried out on a CHI 660D electrochemical working stations (Shanghai Chenhua Instrument, Inc.). All electrochemical performances were carried out in a conventional three-electrode system equipped with platinum electrode and a saturated calomel electrode (SCE) as counter and reference electrodes, respectively. Before electrochemical measurement, we have purged out O_2 from the solution by the inert gas-Ar. The working electrode was made from firstly mixing of active materials, acetylene black, and PTFE (polytetrafluoroethylene) with a weight ratio of 80:15:5, then coating on a piece of foamed nickel foam of about 1 cm^2 , and being pressed into a thin foil at a pressure of 5.0 MPa. The weight of the active sample was about 5 mg. The electrolyte is 3.0 M KOH solution. The

capacitive properties of electrodes were determined by cyclic voltammetry and galvanostatic charge-discharge techniques. Electrochemical impedance spectroscopy measurements of all the samples were conducted at different biased potentials in the frequency range of 100 kHz to 0.01 Hz with AC voltage amplitude of 5 mV by using PARSTAT2273.

3. Results and discussion

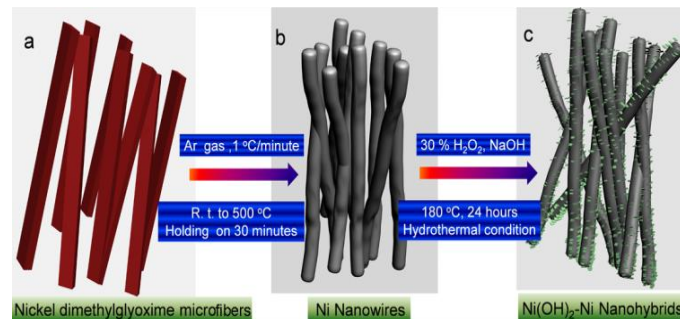


Figure 1 A schematic illustration for the formation of various Ni nanofoams composed of nanowires, and mesoporous $\text{Ni}(\text{OH})_2\text{-Ni}$ nanohybrids.

Figure 1 presents a schematic illustration for the formation of various Ni nanofoams composed of nanowires and mesoporous $\text{Ni}(\text{OH})_2\text{-Ni}$ nanohybrids from $\text{Ni}(\text{DMG})_2$ microfiber precursors. After the $\text{Ni}(\text{DMG})_2$ microfiber precursor was calcined at 500°C in Ar, porous Ni nanowire foams (denoted P1) can be obtained. In **Figure 2**, the XRD analysis confirms that the $\text{Ni}(\text{DMG})_2$ microfiber precursor has been completely transformed to pure Ni (JCPDS-040850). The XRD peaks are broad, indicating that the Ni nanocrystallites are in the nanometer range. $\text{Ni}(\text{OH})_2\text{-Ni}$ nanohybrids (denoted P2) can be obtained by treating the Ni nanowire foams in alkaline H_2O_2 solution under hydrothermal condition. Corresponding XRD patterns are shown in Figure 1, it is seen that the # mark is indexed to $\text{Ni}(\text{OH})_2$ (JCPDS-140117). However, the strongest peak is indexed to pure Ni (JCPDS-040850) due to the existence of central Ni.

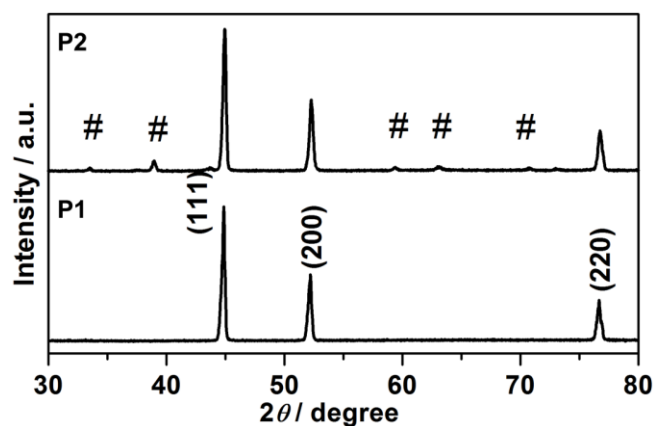


Figure 2 XRD patterns of P1, Ni nanowire foams; and P2, mesoporous $\text{Ni}(\text{OH})_2\text{-Ni}$ nanohybrids, and the # sign is indexed to $\text{Ni}(\text{OH})_2$ (JCPDS-140117).

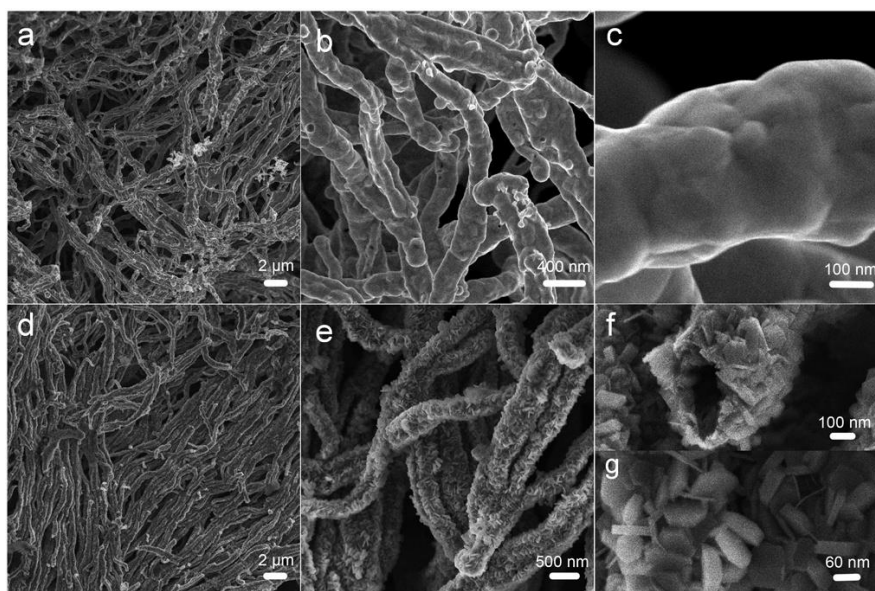


Figure 3 FESEM images of (a-c) P1, Ni nanowire foams; and (d-g) P2, mesoporous Ni(OH)₂-Ni nanohybrids.

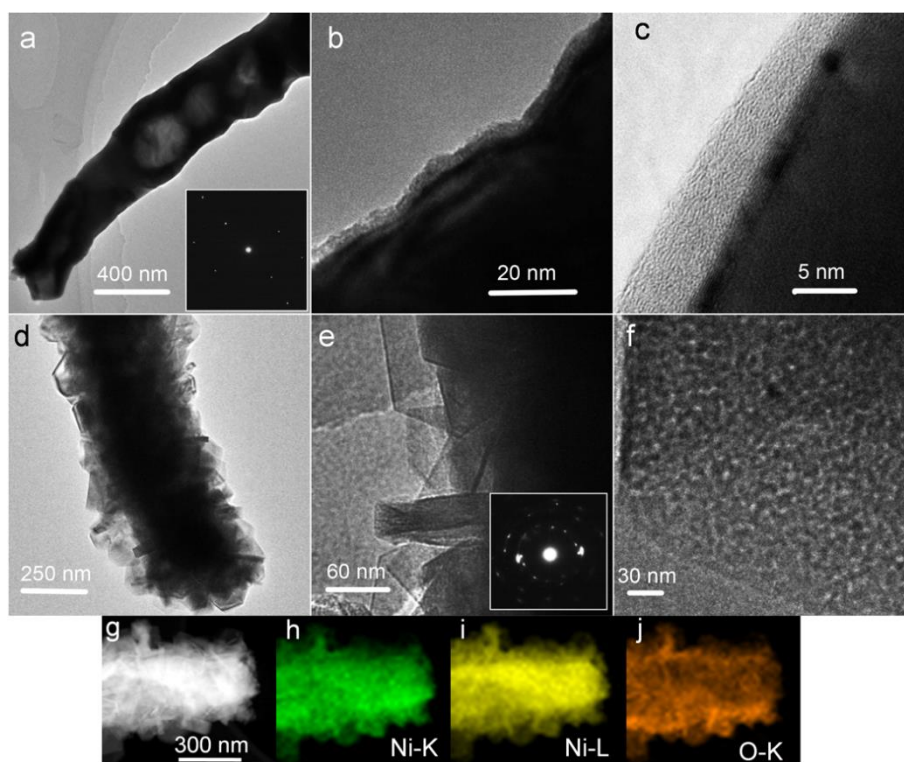


Figure 4 TEM images of (a-c) P1, Ni nanowire foams; and (d-g) P2, mesoporous Ni(OH)₂-Ni nanohybrids, in inset of e, corresponding SAED patterns; (g) STEM HAADF image of P2; (h-j) Corresponding EDX-elemental mapping images of g.

FESEM images of as-prepared samples are shown in **Figure 3**. In Figure 3a, one-dimensional morphology has been maintained, and some Ni nanowires have intertwined with each other. Unlike the Ni(DMG)₂ microfiber precursor, the diameter of Ni nanowires is ~350 nm in Figure 3b, which is narrower than that of the Ni(DMG)₂ microfiber. The surface of Ni nanowires seems smooth in the high magnification FESEM image (Figure 3c). In Figure 3d, it is clear that P2 has the one-dimensional morphology. And some nanowires assemble into big bundles. More importantly, there are many nanoplates on the surface of the one-dimensional structure. And the diameter of a single Ni(OH)₂-Ni nanohybrid is ~500 nm, which is wider than the Ni nanowire due to the formation of Ni(OH)₂ nanoplates (Figure 3e). Some Ni(OH)₂-Ni nanohybrids have the tube-like morphology as shown in Figure 3f. From Figure 3g, the size of a single nanoplate is determined to be ~60 nm.

To better illustrate the structure and porosity, representative TEM images taken from the as-prepared samples are given in **Figure 4**. In **Figure 4a**, the Ni nanowire shows the hollow or semi-hollow structure and its corresponding SAED pattern is shown in the inset of **Figure 4a**. The end of a single Ni nanowire is further magnified in **Figure 4b**. It is clear that the Ni nanowire has good crystallinity, and thus possesses good electron transfer ability because nearly perfect crystal shows little inner resistance. In the higher magnification image (**Figure 4c**), there is an amorphous layer on the fringe of the Ni nanowire. The TEM result shows there are many Ni(OH)₂ nanoplates formed on the Ni nanowire foams (**Figure 4d**) after hydrothermal treatment in alkaline H₂O₂ solution. The Ni(OH)₂ nanoplate is the polycrystalline in nature, which is further proved by its corresponding SAED in inset of **Figure 4e**. More importantly, at higher magnification, there can be found a lot of nanopores on the nanoplates (**Figure 4f**). It is well known that mesopores play critical roles in electrochemical processes, due to their capability of facilitating mass diffusion/transport (e.g., electrolyte penetration and ion transport) and ensuring a high electroactive surface area. To illustrate the spatial distribution of Ni(OH)₂ and Ni in the composite, the elemental mapping is performed on a representative Ni(OH)₂-Ni nanohybrids (**Figure 4g**) under TEM observation. The elemental mapping results (**Figure 4h-j**) demonstrate the generally uniform distribution of O and Ni within the nanohybrid.

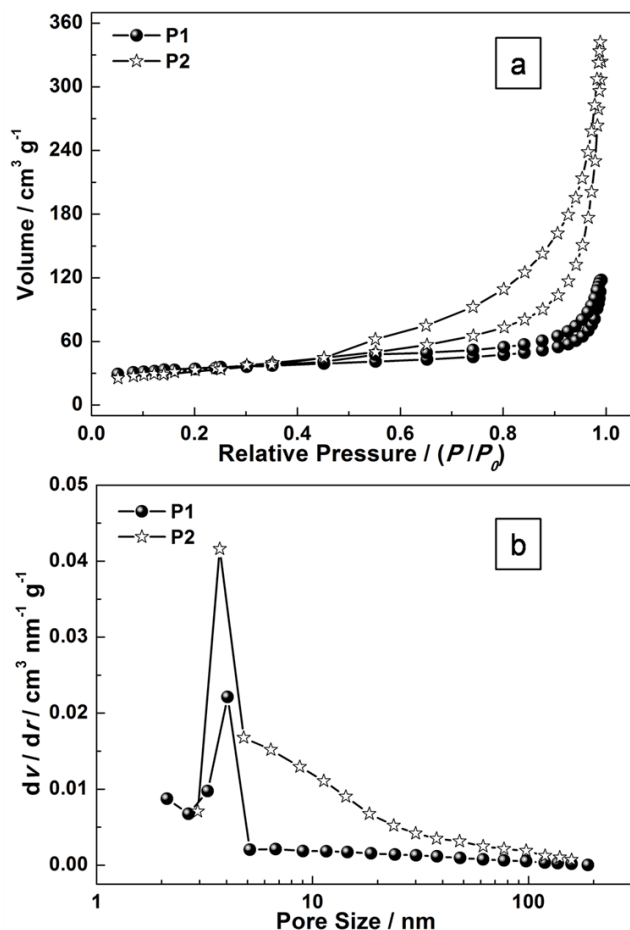


Figure 5 (a) N₂ adsorption-desorption isotherms of as-prepared samples (P1 and P2); and (b) The pore-size distribution curves.

To gain further insight into the specific surface area of the as-prepared sample, Brunauer-Emmett-Teller (BET) measurements were performed. And the N₂ adsorption-desorption isotherms of P1 and P2 were shown in **Figure 5**. The BET surface area is 89.8 m² g⁻¹ (P1) and 151.6 m² g⁻¹ (P2) respectively (**Figure 5**). The pore-size distribution (in **Figure 5b**) was determined by using the Barrett-Joyner-Halenda (BJH) method from the desorption branch of the isotherm. The average pore diameter of the P1 is around 4.5 nm which may result from the intertwined hollow or semi-hollow structures and the amorphous fringe of P1, while that of P2 is around 3.2 nm which may result from the mesoporous morphology of Ni(OH)₂ nanoplates. As widely reported, an effective surface area usually offers many nanochannels for the electrolyte or ions to contact with the surface or interfaces of nanoporous micro/nanostructures.

In order to determine the electrochemical capacitive properties of Ni(OH)₂-Ni nanohybrids, cyclic voltammetry experiments within the 0.0-0.5 V range at a scan rate from 5 to 50 mV s⁻¹ were performed on the mesoporous Ni(OH)₂-Ni nanohybrid electrode in 3.0 M KOH electrolyte at room temperature (**Figure S4**). The shape of the CV curves indicates the pseudocapacitive characteristics of the Ni(OH)₂-Ni nanohybrids samples. Rate capability is one of the important factors for evaluating the power applications of supercapacitors. The discharge curves of the Ni(OH)₂-Ni nanohybrid electrode at different current densities are shown in **Figure 6a**. The discharge curves with an apparent plateau are consistent with the CV results. To calculate the specific capacitance during the galvanostatic charge-discharge processes, the following equation is applied:³⁰

$$C = \frac{i \cdot \Delta t}{m \cdot \Delta V} \quad (1)$$

Where *m* is the mass of electroactive materials (g), ΔV is the range of charge/discharge (V), and *i* is the discharge current (A) applied for time Δt (s).

Figure 6b gives the specific capacitance derived from galvanostatic discharge processes of the mesoporous Ni(OH)₂-Ni nanohybrid electrode at different current densities. The mesoporous Ni(OH)₂-Ni nanohybrid electrode generally exhibits a high specific capacitance and excellent rate capability. At a relatively low current density of 1.25 A g⁻¹, the mesoporous Ni(OH)₂-Ni nanohybrid electrode delivers a high capacitance of 1793 F g⁻¹. Even when the current density is increased by 10 fold, namely 12.5 A g⁻¹, the values remain as high as 850 F g⁻¹.

In view of the high capacitance and excellent rate capability, we further calculate the energy and power densities, specific energy and specific power which are two key factors for evaluating the power applications of electrochemical supercapacitors. A good electrochemical supercapacitor can provide high energy density and high specific capacitance. Specific energy (*E*) and specific power (*P*) derived from GV tests can be calculated from the following equations:³⁰

$$E = \frac{1}{2} C \Delta V^2 \quad (2)$$

$$P = \frac{E}{\Delta t} \quad (3)$$

Where *E* (Wh kg⁻¹), *C* (F g⁻¹), ΔV (V), *P* (W kg⁻¹) and Δt are the specific energy, specific capacitance, the range of the charge/discharge, specific power and discharge time, respectively.

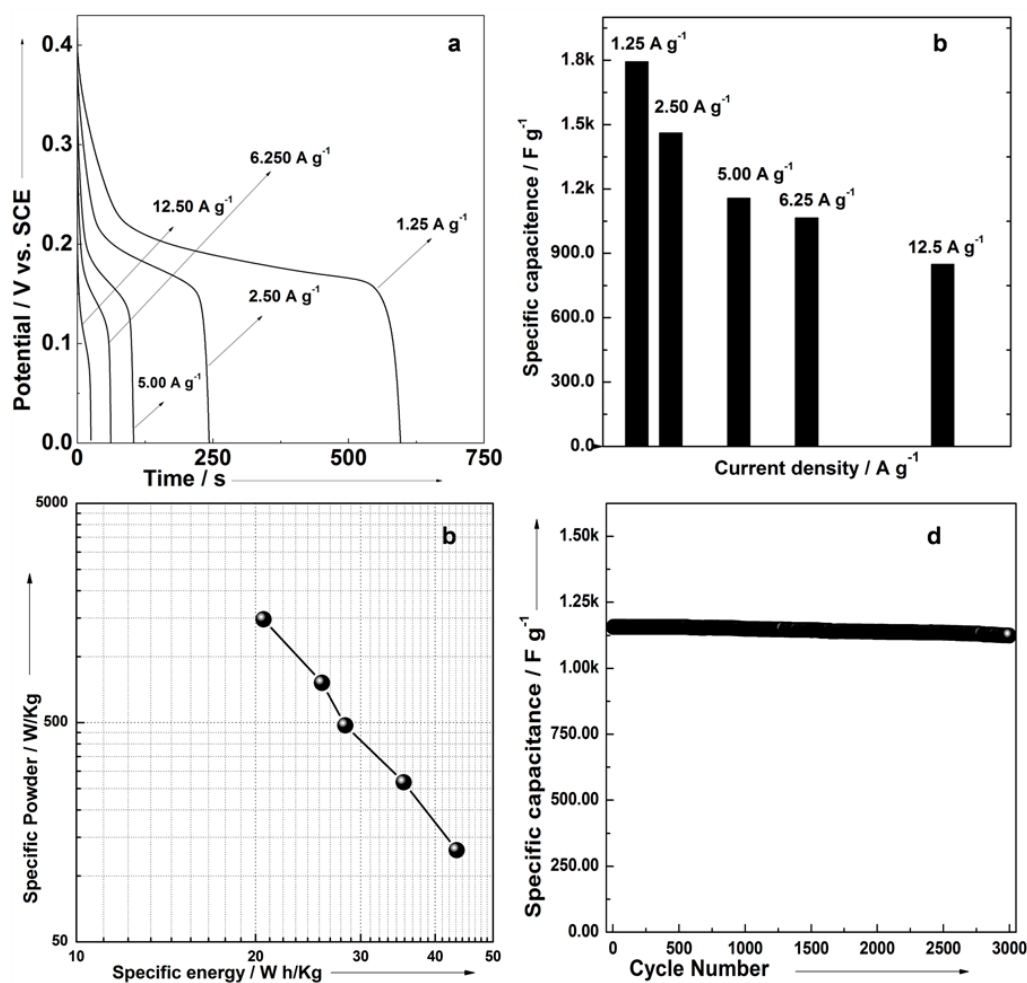


Figure 6 (a) The galvanostatic discharge curves of P2 electrodes during current densities were 1.25–12.5 A g⁻¹ in 3.0 M KOH electrolytes; (b) Specific capacitances of P2 derived from the discharging curves at the current density of 1.25–12.5 A g⁻¹ in 3.0 M KOH electrolytes; (c) A plot of the estimated specific energy and specific power at various charge/discharge rates in 3.0 M KOH electrolytes, and (d) Charge/discharge cycling test at the current density of 5.0 A g⁻¹ in 3.0 M KOH electrolytes.

Figure 6c shows the plot of specific energy and specific power for the mesoporous Ni(OH)₂-Ni nanohybrid electrode in 3.0 M KOH aqueous solution. The specific energy of the mesoporous Ni(OH)₂-Ni nanohybrid electrode decreases from 43.5 to 20.6 Wh kg⁻¹, while the specific power increases from 131 to 1478 W kg⁻¹. The good power density and energy density of mesoporous Ni(OH)₂-Ni nanohybrid nanostructures make it a promising candidate for the electrode materials of supercapacitors. The cyclic stability of the mesoporous Ni(OH)₂-Ni nanohybrid electrode is further evaluated under galvanostatic charge–discharge conditions (Figure 6d). It can be seen that only a very small capacitance drop is observed during the course of prolonged cycling. For example, the specific capacitance remains 98.4% of its initial value after 2000 cycles, and 97.2% after 3000 cycles, revealing its excellent cycling stability.

To identify the exact electrical conductivity of the electrode, we measured electrochemical impedance spectra (EIS) for the mesoporous Ni(OH)₂-Ni nanohybrid electrode in 3.0 M KOH at room temperature under different biased potentials in the frequency range 0.01–10⁵ Hz as shown in Figure 7. As seen in Figure 7, the impedance plot at 0.40 V in 3.0 M KOH exhibits a line with a slope close to 70° along the imaginary axis (Z''), and this is characteristic of an ideally polarizable electrode. At a potential of 0.6 or 0.8 V, the

linear characteristic disappeared. Thus, the proper potential range, over which electrode can generate desirable capacitance, is ≤ 0.40 V. Such superior rate capability of the mesoporous Ni(OH)₂-Ni nanohybrid electrode might be attributed to many reasons: the key one is to cause changes to the many paths of electrons, ions or electrolytes. For example, 1) the highly accessible surface area for mesoporous Ni(OH)₂ structures; 2) the conductivity of the one one-dimensional inner Ni nanostructures. Different surface–interface characteristics and conductivity might have different physicochemical adsorption–desorption abilities towards the ion and diffusion paths of ions, resulting in different electrochemical activities. It is worth mentioning that the abundant mesopores are of great significance for the electrochemical processes.^{11, 33, 36, 37} The highly mesoporous framework allows the facile penetration of the electrolyte that promotes the surface and near surface redox reactions, and guarantees a relatively high electroactive surface area. Thus high specific capacitance can be obtained even at high rates. This could also satisfactorily explain the superior performance of the mesoporous Ni(OH)₂-Ni nanohybrid sample with abundant mesopores.

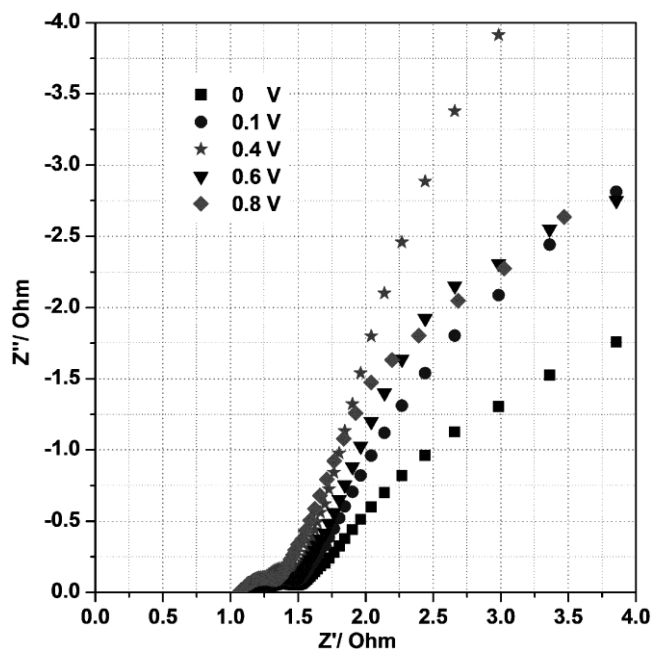


Figure 7 Electrochemical impedance spectra of the P2 electrode at different potentials under room temperature in 3.0 M KOH solution.

4. Conclusions

In summary, we demonstrate the facile synthesis of mesoporous Ni(OH)₂-Ni nanohybrid with excellent supercapacitive performance. The Ni(DMG)₂ microfiber is synthesized as the precursor via a rapid precipitation method at room temperature, followed by controlled annealing to obtain Ni nanowire foams. Moreover, mesoporous Ni(OH)₂-Ni nanohybrids can be obtained by treating the Ni nanowire foams in alkaline H₂O₂ solution under hydrothermal condition. It is found that mesoporous Ni(OH)₂-Ni nanohybrids possesses more abundant mesopores and a higher BET surface area, and exhibits excellent supercapacitive performance in aqueous alkaline electrolytes. The remarkable electrochemical performance is likely due to the desirable nanohybrid and the unique mesoporous nanostructure. We also anticipate that the present synthetic strategy would be adopted to fabricate and optimize other promising nanohybrid materials for various applications.

Acknowledgements

This work is supported by the Program for New Century Excellent Talents of the University in China (grant no. NCET-13-0645), National Natural Science Foundation of China (NSFC-21201010, U1304504). Program for Innovative Research Team (in Science and Technology) in University of Henan Province (14IRTSTHN004). The Science & Technology Foundation of Henan Province (122102210253, 13A150019), and the China Postdoctoral Science Foundation (2012M521115).

Notes and references

^a College of Chemistry and Chemical Engineering, Anyang Normal University, Anyang, 455002, Henan, P. R. China.

^b State Key Laboratory of Coordination Chemistry, Nanjing University, Nanjing, 210093, Jiangsu, P. R. China.

^c E-mail: huanpangchem@hotmail.com

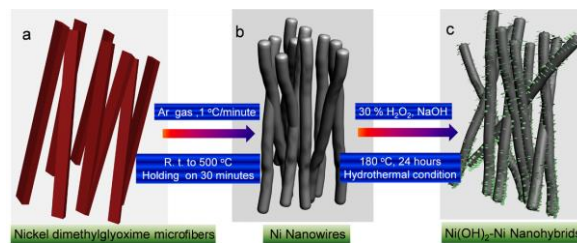
Homepage: <http://huanpangchem.wix.com/advanced-materia>

† Electronic Supplementary Information (ESI) available: See DOI: 10.1039/b000000x/

- X. Peng, L. L. Peng, C. Z. Wu and Y. Xie, *Chem. Soc. Rev.*, 2014, **43**, 3303-3323.
- Y. G. Wang and Y. Y. Xia, *Electrochim. Acta*, 2006, **51**, 3223-3227.
- X. H. Wang, J. J. Ding, S. W. Yao, X. X. Wu, Q. Q. Feng, Z. H. Wang and B. Y. Geng, *J. Mater. Chem. A*, 2014, **2**, 15958-15963
- D. D. Zhu, Y. D. Wang, G. L. Yuan and H. Xia, *Chem. Commun.*, 2014, **50**, 2876-2878
- S. Gu, R. Cai, T. Luo, Z. W. Chen, M. W. Sun, Y. Liu, G. H. He and Y. S. Yan, *Angew. Chem. Int. Ed.*, 2009, **48**, 6499-6502.
- Q. F. Wang, X. F. Wang, J. Xu, X. Ouyang, X. J. Hou, D. Chen, R. M. Wang and G. Z. Shen, *Nano Energy*, 2014, **8**, 44-51.
- D. Zhou, X. R. Su, M. Boese, R. M. Wang and H. Z. Zhang, *Nano Energy*, 2014, **5**, 52-59.
- C. Zhang, H. Yin, M. Han, Z. Dai, H. Pang, Y. Zheng, Y. Q. Lan, J. Bao and J. Zhu, *ACS Nano*, 2014, **8**, 3761-3770.
- K. H. Chang, C. C. Hu and C. Y. Chou, *Chem. Mater.*, 2007, **19**, 2112-2119.
- C. C. Hu, K. H. Chang, M. C. Lin and Y. T. Wu, *Nano Lett.*, 2006, **6**, 2690-2695.
- C. Y. Cao, W. Guo, Z. M. Cui, W. G. Song, W. Cai, *J. Mater. Chem.*, 2011, **21**, 3204-3209.
- Z. Y. Lu, Z. Chang, J. F. Liu and X. M. Sun, *Nano Res.*, 2011, **4**, 658-665.
- M. W. Xu, S. J. Bao and H. L. Li, *J. Solid State Electrochem.*, 2007, **11**, 372-377.
- X. Sun, G. K. Wang, J. Y. Hwang and J. Lian, *J. Mater. Chem.*, 2011, **21**, 16581-16588.
- X. J. Zhang, W. H. Shi, J. X. Zhu, W. Y. Zhao, J. Ma, S. Mhaisalkar, T. L. Maria, Y. H. Yang, H. Zhang, H. H. Hng and Q. Y. Yan, *Nano Res.*, 2010, **3**, 643-652.
- H. Jiang, T. Zhao, C. Z. Li and J. Ma, *J. Mater. Chem.*, 2011, **21**, 3818-3823.
- H. L. Wang, H. S. Casalongue, Y. Y. Liang and H. J. Dai, *J. Am. Chem. Soc.*, 2010, **132**, 7472-7477.
- Y. Gao, J. H. Zhao, Z. Run, G. Zhang and H. Pang, *Dalton Trans.*, 2014, **43**, 17000-17005.
- S. B. Yang, X. L. Wu, C. L. Chen, H. L. Dong, W. P. Hu and X. K. Wang, *Chem. Commun.*, 2012, **48**, 2773-2275.
- H. Pang, Y. Ma, G. Li, J. Chen, J. Zhang, H. Zheng and W. Du, *Dalton Trans.*, 2012, **41**, 13284-13291.
- R. B. Rakhi, W. Chen, D. Cha and H. N. Alshareef, *Nano Lett.*, 2012, **12**, 2559-2567
- C. Z. Yuan, L. Yang, L. R. Hou, L. F. Shen, X. G. Zhang and X. W. Lou, *Energy Environ. Sci.*, 2012, **5**, 7883-7888.
- B. Wang, T. Zhu, H. B. Wu, R. Xu, J. S. Chen and X. W. Lou, *Nanoscale*, 2012, **4**, 2145-2149.
- S. K. Meher and G. R. Rao, *J. Phys. Chem. C.*, 2011, **115**, 15646-15654.
- G. Q. Zhang and X. W. Lou, *Sci. Rep.*, 2013, **3**, 1470.
- H. Jiang, J. Ma and C. Z. Li, *Chem. Commun.*, 2012, **48**, 4465-4467.
- H. L. Wang, Q. M. Gao and L. Jiang, *Small*, 2011, **7**, 2454-2459.
- T. Y. Wei, C. H. Chen, H. C. Chien, S. Y. Lu and C. C. Hu, *Adv. Mater.*, 2010, **22**, 347-351.

- 29 H. B. Wu, H. Pang and X. W. Lou, *Energy Environ. Sci.*, 2013, **6**, 3619-3626.
- 30 H. Pang, J. Deng, J. Du, S. Li, J. Li, Y. Ma, J. Zhang and J. Chen, *Dalton Trans.*, 2012, **41**, 10175-10181.
- 31 C. Z. Yuan, J. Li, L. R. Hou, X. G. Zhang, L. F. Shen and X. W. Lou, *Adv. Funct. Mater.*, 2012, **22**, 4592-4597.
- 32 D. D. Zhu, Y. D. Wang, G. L. Yuan and H. Xia, *Chem. Commun.*, 2014, **50**, 2876-2878.
- 33 M. J. Deng, P. J. Ho, C. Z. Song, S. A. Chen, J. F. Lee, J. M. Chen and K. T. Lu, *Energy Environ. Sci.*, 2013, **6**, 2178-2185
- 34 X. H. Tang, H. J. Li, Z. H. Liu, Z. Yang and Z. L. Wang, *J. Power Sources.*, 2011, **196**, 855-859.
- 35 L. -Q. Mai, F. Yang, Y. -L. Zhao, X. Xu, L. Xu and Y. -Z. Luo, *Nature Commun.*, 2011, **2**, 318.
- 36 Z. S. Wu, W. C. Ren, D. W. Wang, F. Li, B. L. Liu and H. -M. Cheng, *ACS Nano*, 2010, **4**, 5835-5842.
- 37 Q. Li, Z. Wang, G. Li, R. Guo, L. Ding and Y. Tong, *Nano Lett.*, 2012, **12**, 3803-3807.
- 38 W. F. Wei, X. W. Cui, W. X. Chen and D. G. Ivey, *Chem. Soc. Rev.*, 2011, **40**, 1697-1721.
- 39 H. Pang, S. M. Wang, G. C. Li, Y. H. Ma, J. Li, X. X. Li, L. Zhang, J. S. Zhang and H. H. Zheng, *J. Mater. Chem. A.*, 2013, **1**, 5053-5060.
- 40 J. R. Zhang, D. C. Jiang, B. Chen, J. J. Zhu, L. P. Jiang and H. Q. Fang, *J. Electrochem. Soc.*, 2001, **148**, 1362-1367.
- 41 Y. F. Yan, Q. L. Cheng, G. C. Wang and C. Z. Li, *J. Power Sources*, 2011, **196**, 7835-7840.
- 42 J. Ren, L. Li, C. Chen, X. L. Chen, Z. B. Cai, L. B. Qiu, Y. G. Wang, X. G. Zhu and H. S. Peng, *Adv. Mater.*, 2013, **25**, 1155-1159.
- 43 S. W. Lee, J. Kim, S. Chen, P. T. Hammond and Y. Shao-Horn, *ACS Nano.*, 2010, **4**, 3889-3896.
- 44 Y. Zhao, C. G. Hu, Y. Hu, H. H. Cheng, G. Q. Shi and L. T. Qu, *Angew. Chem. Int. Ed.*, 2012, **124**, 11533-11537.
- 45 X. Y. Lang, A. Hirata, T. Fujita and M. W. Chen, *Nat. Nanotechnol.*, 2011, **6**, 232-236.
- 46 Q. Lu, M. W. Lattanzi, Y. P. Chen, X. M. Kou, W. F. Li, X. Fan, K. M. Unruh, J. G. Chen and J. Q. Xiao, *Angew. Chem., Int. Ed.*, 2011, **50**, 1-5.
- 47 G. X. Pan, X. Xia, F. Cao, P. S. Tang and H. F. Chen, *Electrochim. Acta.*, 2012, **63**, 335-340.
- 48 M. Hasan, M. Jamal and K. M. Razeeb, *Electrochim. Acta.*, 2012, **60**, 193-200.
- 49 M. Salari, S. H. Aboutalebi, K. Konstantinov and H. K. Liu, *Phys. Chem. Chem. Phys.*, 2011, **13**, 5038-5041.
- 50 Z. Lu, Z. Chang, W. Zhu, X. M. Sun, *Chem. Commun.*, 2011, **47**, 9651-9653.
- 51 G. W. Yang, C. L. Xu, H. L. Li, *Chem. Commun.*, 2008, **44**, 6537-6539.
- 52 U. M. Patil, K. V. Gurav, V. J. Fulari, C. D. Lokhande and O. S. Joo, *J. Power Sources*, 2009, **188**, 338-342.
- 53 L. C. Wu, Y. J. Chen, M. L. Mao, Q. H. Li, and M. Zhang, *ACS Appl. Mater. Interfaces*, 2014, **6**, 5168-5174
- 54 B. L. Hua, X. Y. Qin, A. M. Asiri, K. A. Alamry, A. O. Al-Youbi and X. P. Sun, *Electrochim. Acta* 2013, **107**, 339-342.
- 55 L. Tschugaeff and Ber. Dtsch. Chem. Ges., 1905, **38**, 2520-2522.
- 56 K. Yamamoto, T. Kamata, Y. Yoshida, K. Yase, F. Mizukami and T. Ohta, *Adv. Mater.*, 1998, **10**, 1018-1022.

ToC



Mesoporous nickel hydroxide-nickel nanohybrids are successfully obtained via oxidation of Ni nanowire foams indirectly from coordination microfibers, which are successfully applied as high-performance supercapacitor electrodes.